Preparation and Some Electrical Properties of Yttrium-Doped Antimonic Acids

Kiyoshi Ozawa,* Junhu Wang, Jinhua Ye, Yoshio Sakka, and Muneyuki Amano

National Institute for Materials Science, 1-2-1, Sengen, Tsukuba-shi, Ibaraki 305-0047, Japan

Received October 7, 2002. Revised Manuscript Received December 10, 2002

New kinds of yttrium-doped antimonic acid compounds with the compositional formula of $H_{1-3x}Y_xSbO_3 \cdot nH_2O$ ($0 \le x \le 0.22$, $n = 0.5$) were successfully synthesized by solution processing using the reaction of an aqueous hydrogen peroxide solution with antimony and yttrium alkoxides, i.e., Sb(O-*iso*-$C_3H_7)_3$ and Y(O-*iso*-$C_3H_7)_3$, respectively. It is recognized from TEM measurements that the resulting materials ($x = 0$ and 0.12) consist of fine crystals with a relatively uniform particle size of 40−50 nm. The Rietveld refinement based on X-ray diffraction data revealed that the Y atoms in the materials are present on an interstitial 16d site. The ionic transference numbers and proton conductivity were evaluated using ac and dc measurement methods. Consequently, it was found that the ionic transference numbers are over 0.98 regardless of the yttrium-doping degrees and that the proton conductivity is significantly enhanced by the yttrium doping; the conductivity at 20 °C is 8.3×10^{-5} and 3.8×10^{-3} S cm^{-1}, respectively, for the pure material and the doped material ($x = 0.12$). The activation energies of 0.58 and 0.43 eV in the temperature range of 243−298 K are obtained for the pure material and the doped material ($x = 0.12$), respectively. Such variation in the proton conduction is qualitatively interpreted in terms of the strength of the hydrogen bonding between the oxygen atoms of the ($Sb_2O_6^{2-}$) frameworks and H_2O or H_3O^+ species, which changes according to the yttrium doping.

Introduction

Recently, some metal hydrous oxides with a high proton conductivity such as $ZrO_2 \cdot nH_2O$ and $WO_3 \cdot nH_2O$ have become of interest as an electrolyte for fuel cells working in the intermediate temperature range of 100−300 °C.[1,2] At present, the perfluorinated ion-exchange membrane (Nafion) is exclusively used as the electrolyte,[3,4] and considerable efforts have been devoted to it during the past few years. In fact, Nafion has the high proton conductivity of 10^{-2} S cm^{-1} at room temperature;[5,6] however, there are some disadvantages derived from the polymer itself. It suffers from a low operating temperature such as below 100 °C and from permeability by many kinds of organic solvents.[7] Moreover, its high cost is still prohibitive for wide commercial applications. Therefore, the preparation of materials as a substitute for Nafion is now being realized.

For antimonic acids ($HSbO_3 \cdot nH_2O$ or $Sb_2O_5 \cdot nH_2O$), there are structurally three polymorphous types: cubic (pyrochlore-type), monoclinic, and amorphous.[8,9] It is known that the pyrochlore-type antimonic acid has a relatively high proton conductivity of $\sim 10^{-4}$ S cm^{-1} at room temperature.[10] In general, pyrochlore-type compounds are represented by the formula $A_2M_2O_6O'$ and correspond to space group symmetry of $Fd\bar{3}m$.[11] As shown in Figure 1, this structure is characterized by a three-dimensional ($M_2O_6^{n-}$) framework built up of vertex-linked MO_6 octahedra. In this framework, there are interconnected channels with large cavities (8 per unit cell).[11] For the pyrochlore-type antimonic acid, A = H or H_3O, M = Sb, and O′ can be replaced by H_2O. Slade et al.[12] have revealed that the full structure at ambient temperature is assumed to be $H_{0.72}(H_3O)_{0.28}SbO_3 \cdot 0.22H_2O$ from the Rietveld refinement using neutron diffraction data.

Between the three different H species in the pyrochlore-type antimonic acid, there is the following equilibrium:[12,13]

$$Sb{-}OH + H_2O \rightleftarrows Sb{-}O^- + H_3O^+ \qquad (1)$$

The proton conduction occurs by the Grotthuss mech-

* To whom correspondence should be addressed. Telephone: +81-298-59-2456. Fax: +81-298-59-2401. E-mail: OZAWA.Kiyoshi@nims.go.jp

(1) Honma, I.; Takeda, Y.; Bae, J. M. *Solid State Ionics* **1999**, *120*, 255.
(2) Li, Y. M.; Hibino, T.; Miyayania, M.; Kudo, T. *Solid State Ionics* **2000**, *134*, 271.
(3) Depre, L.; Ingram, M.; Poinsignon, C.; Popall, M. *Electrochim. Acta* **2000**, *45*, 1337.
(4) Zawadzinski, T. A., Jr.; Derouin, C.; Radzinski, S.; Sherman, R. T.; Smith, V. T.; Springer, T. E.; Gottesfeld, S. *J. Electrochem. Soc.* **1993**, *140*, 1041.
(5) Kreuer, K. D. *Chem. Mater.* **1996**, *8*, 610.
(6) Colomban, Ph., Ed. *Proton Conductors: Solids membrance and gel-material and devices*; Cambrige University Press: Cambrige, 1992.
(7) Colomer, M. T.; Anderson, M. A. *J. Non-Cryst. Solids* **2001**, *290*, 93
(8) Chitrakar, R.; Abe, M. *Mater. Res. Bull.* **1988**, *23*, 1231.
(9) Abe, M.; Ito, T. *Bull. Chem. Soc. Jpn.* **1968**, *41*, 333.
(10) England, W. A.; Cross, M. G.; Hamnett, A.; Wiseman, P. J.; Goodenough, J. B. *Solid State Ionics* **1980**, *1*, 231.
(11) Wells, A. F. *Structural Inorganic Chemistry*; Clarendon Press: Oxford, 1984.
(12) Slade, R. C. T.; Hall, G. P.; Ramanan, A.; Prince, E. *Solid State Ionics* **1996**, *92*, 171.

10.1021/cm020990i CCC: $25.00
Published on Web 01/22/2003

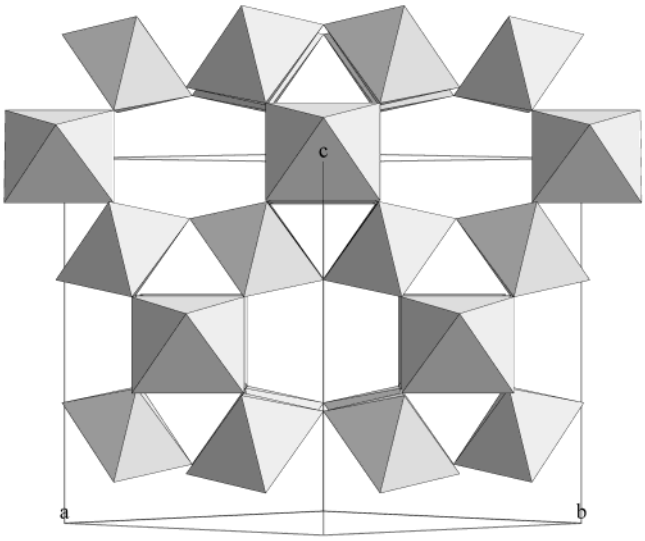

Figure 1. Three-dimensional ($M_2O_6^{n-}$) framework built up of vertex-linked MO_6 octahedra in the cubic pyrochlore structure.

anism (or translocation) between the H_3O^+ and H_2O species.[6,12,13] A number of studies have been devoted to the proton conduction of the pyrochlore-type antimonic acid or related compounds over the past 2 decades. To our knowledge, however, there is no report in which the proton conductivity is remarkably enhanced so as to cope with the industrial demand such as over 10^{-2} S cm^{-1} at ambient temperature. Taking into account the compositional flexibility of the structure, various conductivities can be expected for the pyrochlore-type antimonic acid due to chemical substitution or insertion. Indeed, with respect to the chemical substitution, Riviere et al.[14] reported the $H_{2x}Sb_{2x}W_{2-2x}O_6 \cdot nH_2O$ ($x = 0.5-1.0$) compounds. However, its proton conductivity shows a lower value as compared to that of the pure material.

From this point of view, we have prepared yttrium-doped antimonic acids, and recently, it was found that the proton conductivity of the materials is significantly enhanced.

In this paper, we first describe the preparation of the yttrium-doped antimonic acids and their structural characterization. Second, we discuss some electrical properties of the materials, that is, the ionic transference numbers and the proton conductivity.

Experimental Section

Preparation Procedure. The yttrium-doped antimonic acids were prepared by solution processing using the direct reaction of an aqueous hydrogen peroxide (H_2O_2) solution with the antimony and yttrium alkoxides: $Sb(O\text{-}iso\text{-}C_3H_7)_3$ and $Y(O\text{-}iso\text{-}C_3H_7)_3$ (>99.9%, Kojundo Chemical Lab. Co.). As reported by Kudo and co-workers,[15,16] in this procedure, peroxo-polymetallic acids with the peroxo groups of M−O−O−M′ (M and M′: metals) may be produced as precursors. These alkoxides were proportionally weighed for the Y/Sb molar ratios (the yttrium-doping degrees) of 0−0.3. Each quantity of $Y(O\text{-}iso\text{-}C_3H_7)_3$ was dissolved in a small amount of 2-ethoxyethanol ($C_2H_5OCH_2CH_2OH$, >99%, Aldrich) and mixed with $Sb(O\text{-}iso\text{-}C_3H_7)_3$. These mixtures were added in limited amounts to a 30% H_2O_2 aqueous solution and then refluxed at ∼100 °C for over 3 h that produced translucent white sols. Subsequently, the excess H_2O_2 in the sols was catalytically decomposed using several platinum foils, and the organic residue was removed by extraction with diethyl ether. Finally, the sols were dried by evaporation at 120 °C to give the yttrium-doped antimonic acid powders. The resulting powders were held for more than 24 h at the saturated water vapor pressure and at the temperature of 20 °C and then used for the following characterization and electrical property measurements.

Characterization. To investigate the morphology of the yttrium-doped antimonic acids, transmission electron microscopy (TEM) measurements were done for the materials produced in the sols using a field emission gun transmission electron microscope (JEOL JEM4000EX).

The thermal decomposition behavior was investigated by thermogravimetric analysis (TGA) at the heating rate of 5 °C/min in an argon atmosphere using a Mac Science TGA2000 thermal analyzer. The specific areas were estimated using the BET equation based on the adsorbed areas of the nitrogen molecules. The Y/Sb molar ratios and $Sb^{3+}/(Sb^{5+} + Sb^{3+})$ ratios in the resulting powders were determined by atomic adsorption spectroscopy and $KMnO_4$ titration methods,[17] respectively. For the latter method, after the sample powders were dissolved in a 6 mol % HCl aqueous solution, the quantities of the Sb^{3+} ions were determined on the basis of the oxidation reaction of $Sb^{3+} \rightarrow Sb^{5+}$ by titrating a 0.1 mol % $KMnO_4$ aqueous solution.

For the purpose of the identification of the crystalline phase and structure, X-ray diffraction experiments were done at ambient temperature using a rotating cathode X-ray diffractometer (JEOL JDX3500) at 35 kV and 300 mA with graphite-monochromatized Cu Kα radiation ($\lambda = 1.54178$ Å). The lattice parameters were determined by an iterative least-squares procedure using at least six Bragg reflections with 2θ values in the range of 20−75°. The powder X-ray diffraction refinement was performed for the yttrium-doped antimonic acids by the Rietveld method using the RIETAN computational system.[18] For this refinement, the X-ray diffraction data were collected using a $2\theta-\theta$ step-scanning mode in the 2θ range of 10−100° with a step width of 0.02° and a step time of 5 s. For collecting the data, the sample powers were well grounded and attached as lightly as possible on a sample holder.

Electrical Property Measurements. The ionic transference numbers were determined by a simplified polarization method in which polarization−depolarization curves were recorded by applying a 1-V dc bias and cutting it off at the temperature of 20 °C. The proton conductivity was evaluated by an ac impedance method using a Hewlett-Packard 4194 analyzer. For these measurements, compact polycrystalline disks being 13 mm in diameter and ∼1-mm thick and having a constant relative density of ∼60% were used as the samples; the disks were prepared by pressing the resulting powders at 147 MPa. As the electrodes, nickel sponges were attached to both sides of the disks by pressing, and then platinum wires were connected to the nickel sponges using a silver paste. Furthermore, to control and maintain the water content, the disks were held again for more than 24 h at the saturated water vapor pressure and at the temperature of 20 °C and then immediately embedded in an epoxy resin (SpeciFix-20, Struers A/S).[19]

Results and Discussion

Morphology. Figure 2 shows the bright-field TEM images of the yttrium-doped antimonic acid compounds

(13) Colomban, Ph.; Doremieux-Morin, C.; Piffard, Y.; Limage, M. H.; Novak, A. *J. Mol. Struct.* **1989**, *213*, 83.
(14) Riviere, M.; Fourquet, J. L.; Grins, J.; Nygren, M. *Mater. Res. Bull.* **1988**, *23*, 965.
(15) Kudo, T. *Nature* **1984**, *312*, 537.
(16) Nanba, T.; Takano, S.; Yasui, I.; Kudo, T. *J. Solid State Chem.* **1991**, *90*, 47.
(17) Oodan, K.; Umemiya, S.; Yamada, Y. *J. Chem. Soc. Jpn.* **1969**, *72*, 2373.
(18) Izumi, F. In *The Rietveld Method*; Young, R. A. Ed.; Oxford University Press: Oxford, 1993.
(19) Deniard-Courant, S.; Piffard, Y. *Solid State Ionics* **1988**, *27*, 189.

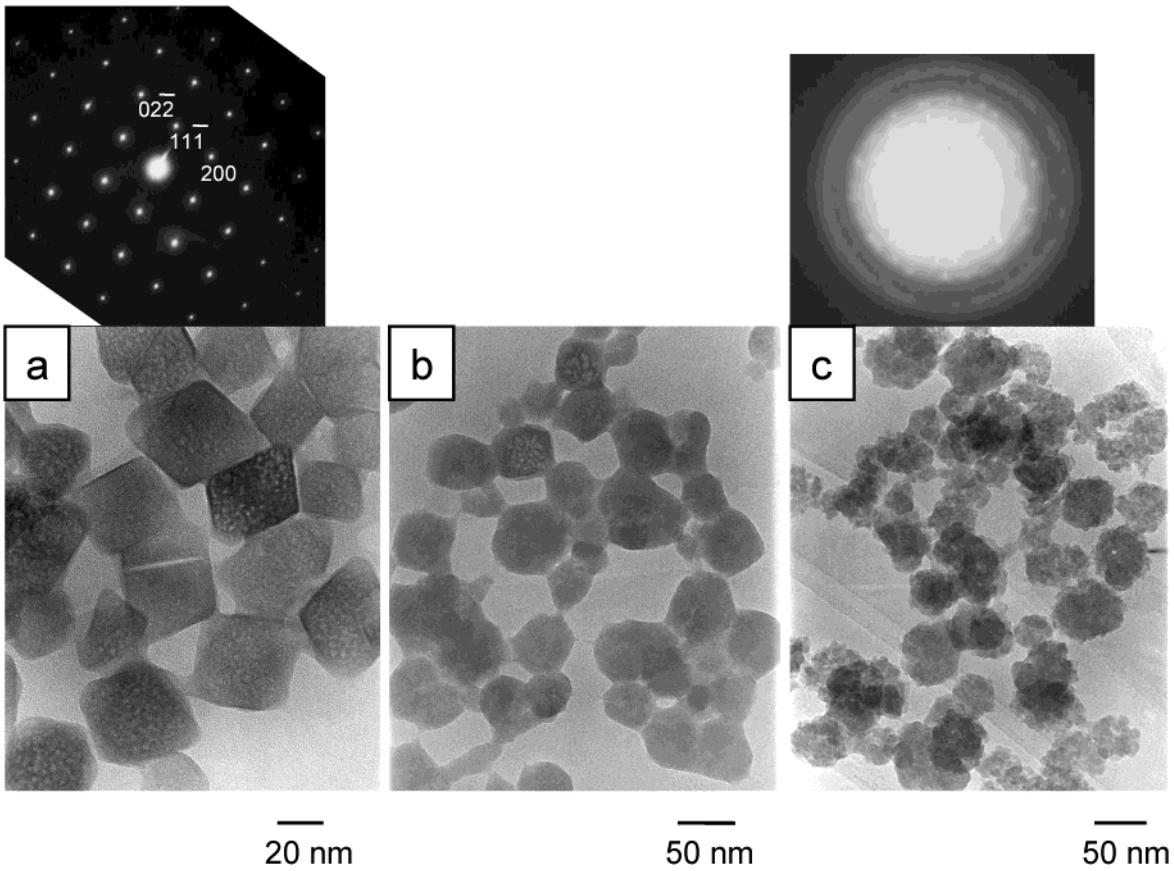

Figure 2. TEM images of the pure material (a) and the yttrium-doped materials for $x = 0.12$ (b) and $x = 0.22$ (c) formed in the sols after the reaction of antimony and yttrium alkoxides with an aqueous hydrogen peroxide solution, together with the selected area electron diffraction images.

having the Y/Sb molar ratios (the x values) of 0, 0.12, and 0.22, formed in the sols after the reaction of an aqueous H_2O_2 solution with the antimony and yttrium alkoxides. Selected area electron diffraction images are also shown in Figure 2. Note that the x values refer to the analytical ones, hereafter. As shown in Figure 2a, the compound for $x = 0$ consists of fine crystals with an octahedral geometry, and the individual crystals characteristically have a relatively uniform particle size of ~50 nm. Its electron diffraction image derived from one particle shows a typical spot pattern of a cubic cell corresponding to the pyrochlore-type antimonic acid. Almost similar morphology, but a somewhat smaller particle size of ~40 nm, can be seen in the compound for $x = 0.12$ in Figure 2b. On the other hand, for the compound material with $x = 0.22$ in Figure 2c, the particles are coated with amorphous material with a very small particle size of below 5 nm, and halo patterns appear in the diffraction image. Such an amorphous material is found to be also present in the interparticle region.

Water Content, Specific Surface Areas, and $Sb^{3+}/(Sb^{5+} + Sb^{3+})$ Ratios. Typical thermogravimetric curves for the yttrium-doped antimonic acids ($x = 0$ and 0.12) are shown in Figure 3; note that the thermogravimetric analyses were carried out immediately after holding the sample powders at the saturated water vapor pressure. It was found that a weight loss occurs in four temperature stages for both compounds ($x = 0$ and 0.12): approximately room temperature to 100 °C, 190−230 °C, 250−500 °C, and 530−620 °C. Such behavior is

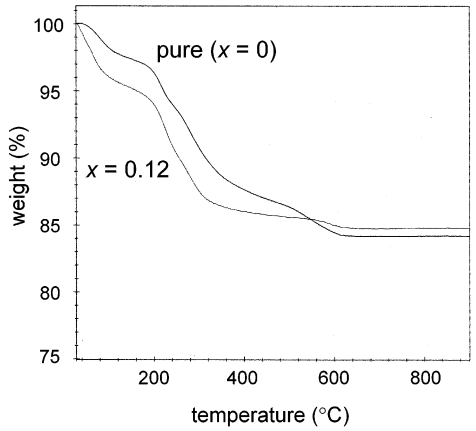

Figure 3. Thermogravimetric analysis plots for the materials ($x = 0$ and 0.12).

almost consistent with the results of Abe and Ito[9] and Riviere et al.,[14] in which a weight loss, due to the release of the surface (and/or interparticle) water and the bulk water, occurs according to the following reactions:

$$HSbO_3 \cdot (n_1 + n_2)H_2O \rightarrow HSbO_3 \cdot n_2H_2O \text{ (at } \sim 250 \text{ °C)} \quad (2)$$

$$HSbO_3 \cdot n_2H_2O \rightarrow HSbO_3 \text{ (at } \sim 350 \text{ °C)} \quad (3)$$

$$HSbO_3 \rightarrow SbO_{2.5} \text{ (at } \sim 530 \text{ °C)} \quad (4)$$

where the n_1 and n_2 values refer to the surface and bulk water contents, respectively. It is also reported that

Table 1. Surface Water Content (n_1), Bulk Water Content (n_2), Specific Surface Areas, and $Sb^{3+}/(Sb^{5+} + Sb^{3+})$ Ratios for the Yttrium-Doped Antimonic Acids ($x = 0$, 0.12, and 0.22)

x (Y/Sb molar ratio from chemical analysis)	water content n: total n_1: surface (and/or interparticle) n_2: bulk	specific area ($m^2\ g^{-1}$)	$Sb^{3+}/(Sb^{5+} + Sb^{3+})$ ratio
0	$n = 1.5$ $n_1 = 0.96$ $n_2 = 0.54$	39.8	0.020
0.12	$n = 1.72$ $n_1 = 1.20$ $n_2 = 0.52$	64.6	0.023
0.22	$n = 2.32$ $n_1 = 1.91$ $n_2 = 0.41$	114.9	

there is a weight loss at the higher temperature of ~600 °C, caused by the release of oxygen molecules according to the following reaction:

$$SbO_{2.5} \rightarrow {}^1/_6Sb_6O_{13} \quad (5)$$

Table 1 lists the surface and bulk water contents (the $n_1$and n_2 values) in the yttrium-doped antimonic acids ($x = 0$, 0.12, and 0.22) estimated from the thermogravimetric curves together with specific surface areas and $Sb^{3+}/(Sb^{5+} + Sb^{3+})$ ratios. The specific surface areas have significantly increased with the increasing x values. Such behavior is considered to result from the enlargement of the amorphous material as mentioned in the TEM results. The $Sb^{3+}/(Sb^{5+} + Sb^{3+})$ ratios are nearly zero between the compounds for $x = 0$ and 0.12, which will be discussed later in connection with the introduction of hydrogen vacancies. It was found that the n_1 values increase from 0.96 to 1.91 with the increasing x values, which are responsible for the increasing specific surface areas. On the other hand, there is no significant difference in the n_2 values; the n_2 value is 0.54 and 0.52, respectively, for $x = 0$ and 0.12. The slightly smaller n_2 value of 0.41 observed for $x = 0.22$ is supposed to seemingly occur because of the significant enlargement of the amorphous material.

The structural requirements correspond to a composition of $HSbO_3 \cdot 0.5H_2O$ (or $Sb_2O_5 \cdot 2H_2O$) for the pyrochlore-type antimonic acid with the maximum bulk water content, as indicated by Slade et al.[12] Thus, taking into account the above thermogravimetric results, it may be concluded that the bulk water content in the yttrium-doped antimonic acids after holding at the saturated water vapor pressure is $n_2 = 0.5$ for a composition of $H_{1-3x}Y_xSbO_3 \cdot n_2H_2O$.

Structural Characterization. Figure 4 shows the X-ray diffraction profiles of the yttrium-doped antimonic acids with various yttrium-doping degrees of $x = 0-0.32$. When the x values are between $x = 0$ and $x = 0.22$, all the Bragg reflections can be assigned to those of the pyrochlore-type antimonic acid. Simultaneously, the reflection lines shift to higher 2θ values and broaden in width with the increasing yttrium-doping degrees; the former behavior refers to the lattice contraction and the latter to the decrease in crystallinity. On the other hand, when the x value is beyond 0.22, the X-ray diffraction profiles drastically transform into that of an amorphous material.

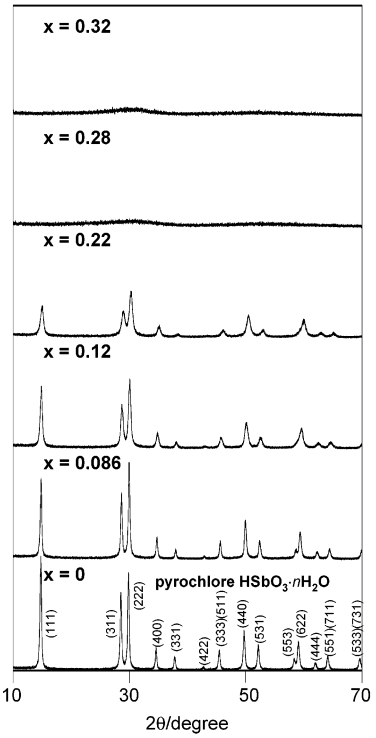

Figure 4. X-ray diffraction profiles of the yttrium-doped antimonic acids with various yttrium-doping degrees of $x = 0-0.32$.

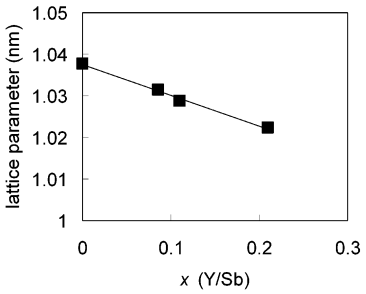

Figure 5. Lattice parameters as a function of x in the yttrium-doped antimonic acids.

In Figure 5, the cubic lattice parameters in the yttrium-doped antimonic acids are plotted as a function of x in the x range of 0−0.22. It was found that the lattice parameters linearly decrease with an increase in the x value. Such variation in the lattice parameters are related to the Y atom position in the structures, as will be discussed in the following section.

In the pyrochlore-type antimonic acid, it is generally accepted that the Sb and O(1) atoms, consisting of the SbO_6 octahedra, are placed on a 16c site (0, 0, 0) and a 48f site (x, $^1/_8$, $^1/_8$), respectively.[10,12,14] In addition, Slade et al.[12] have revealed by neutron powder diffraction refinement that the O(2) atoms of the H_2O or H_3O^+ species are correctly positioned on a 32e site (x, x, x). Except for the 32e site, a 16d site ($^1/_2$, $^1/_2$, $^1/_2$) and an 8b site ($^3/_8$, $^3/_8$, $^3/_8$) are present as interstitial sites in the cavity for the pyrochlore-type antimonic acid.[11,12]

With respect to the chemical substitution of the pyrochlore-type antimonic acid, Riviere et al.[14] reported that part of the Sb atoms are replaced by the W atoms in the $H_{2x}Sb_{2x}W_{2-2x}O_6 \cdot nH_2O$ ($x = 0.5-1.0$) compounds. Such a substitution may be due to the fact that there is no significant difference between the ionic radii of Sb^{5+}

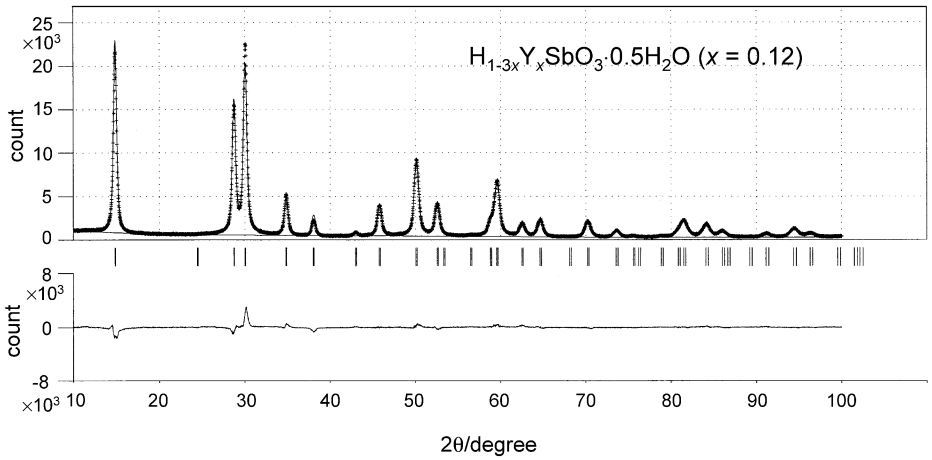

Figure 6. Observed and calculated X-ray diffraction profiles of the as-prepared yttrium-doped antimonic acid ($H_{0.64}Y_{0.12}SbO_3 \cdot 0.5H_2O$) and the crystallographic model.

Table 2. Refined Structural Parameters of $HSbO_3 \cdot 0.5H_2O$ and $H_{1-3x}Y_xSbO_3 \cdot 0.5H_2O$ ($x = 0.12$)'

$HSbO_3 \cdot 0.5H_2O$	$H_{1-3x}Y_xSbO_3 \cdot 0.5H_2O$ ($x = 0.12$)
Space Group	
$Fd\bar{3}m$	$Fd\bar{3}m$
Lattice Parameter	
10.3656(4) Å	10.2881(4) Å
Atomic Position and Isotropic Thermal Parameter	
Sb: 16c (0, 0, 0); occp. = 1, $B = 0.6(3)$ Å^2	Sb: 16c (0, 0, 0); occp. = 1, $B = 0.5$ Å^2
O(1): 48f (x, $^1/_8$, $^1/_8$); occp. = 1, $B = 1$ Å^2, $x = 0.323(3)$	O(1): 48f (x, $^1/_8$, $^1/_8$); occp. = 1, $B = 1$ Å^2, $x = 0.331(2)$
O(2): 32e (x, x, x); occp. = 0.25, $B = 1$ Å^2, $x = 0.553(7)$	O(2): 32e (x, x, x); occp. = 0.25, $B = 1$ Å^2, $x = 0.589(5)$
	Y: 16d ($^1/_2$, $^1/_2$, $^1/_2$); occp. = 0.12, $B = 0.5$ Å^2
R Factor	
$R_{wp} = 0.118$, $R_{exp} = 0.037$, $R_F = 0.027$	$R_{wp} = 0.087$, $R_{exp} = 0.027$, $R_F = 0.025$
Shortest Interatomic Distance	
Sb−O(1): 1.98(1) Å; O(1)−O(1): 2.70(1) Å	Sb−O(1): 2.00(1) Å; O(1)−O(1): 2.65(1) Å
O(1)−O(2): 2.60(1) Å	O(1)−O(2): 2.71(1) Å
	Y−O(1): 2.52(1) Å; Y−O(2): 2.52(1) Å

and W^{6+}; $r(Sb^{5+}) = 0.060$ and $r(W^{6+}) = 0.060$ nm when both the individual coordination numbers (CN) are 6.[20] In contrast, the ionic radius of Y^{3+} is much larger than that of Sb^{5+}; $r(Y^{3+}) = 0.090$ nm for CN = 6.[20] Therefore, taking into account the variation in the lattice parameters, it is reasonable to postulate that the Y atoms in the yttrium-doped antimonic acids are not substituted for the Sb atoms occupying the 16c sites, but placed on an interstitial site. Assuming that the Y atoms are positioned this way since the $Sb^{3+}/(Sb^{5+} + Sb^{3+})$ ratios are nearly zero (Table 1), hydrogen vacancies would be introduced to maintain charge balance, and thus, the compositional formula is suggested to be $H_{1-3x}Y_x$-$SbO_3 \cdot nH_2O$ for the yttrium-doped antimonic acids.

The Rietveld refinement was performed for the yttrium-doped antimonic acids ($x = 0$ and 0.12) with the maximum bulk water content, that is, $HSbO_3 \cdot 0.5H_2O$ and $H_{0.64}Y_{0.12}SbO_3 \cdot 0.5H_2O$. In the refinement, the space group $Fd\bar{3}m$ was selected, and the positions for the Sb, O(1), and O(2) atoms were fixed at 16c, 48f, and 32e, respectively. The Y atom position was then fixed at 16d. Indeed, except for the 16d site, the Y atom position can be assumed to be 32e or 8b; however, it was found that such positioning led to poorer convergence in the refinement. Next, the occupancy factor of each site was fixed according to the compositional formula of $H_{1-3x}Y_x$-$SbO_3 \cdot nH_2O$. For example, in the case of $H_{0.64}Y_{0.12}$-$SbO_3 \cdot 0.5H_2O$, the occupancy factor was fixed at 1.0, 0.12, 1.0, and 0.25, respectively, for the 16c (Sb), 16d (Y), 48f (O(1)), and 32e (O(2)) sites, where the occupancy factor of 0.25 for the 32e site corresponds to 0.5 O(2) atoms per formula unit cell. Furthermore, the individual isotropic thermal parameters (B values) were fixed except for that of the Sb atom in the case of $HSbO_3 \cdot 0.5H_2O$ because they became negative due to their correlation with other parameters. Figure 6 shows the observed and calculated X-ray diffraction profiles of the as-synthesized yttrium-doped antimonic acid ($H_{0.64}Y_{0.12}$-$SbO_3 \cdot 0.5H_2O$) and its crystallographic model. The final results of the refinement are summarized in Table 2. It should be noted that a good minimization of the difference is obtained with good reliability factors: $R_{wp} = 0.087$, $R_{exp} = 0.027$, and $R_F = 0.025$ for $H_{1-3x}Y_xSbO_3 \cdot 0.5H_2O$ ($x = 0.12$). The results of the Rietveld refinement ensure the validity of the model structure.

As shown in Figure 7, the 16d site, that is, the Y atom position, is at the center of the so-called cavity window. For this structure, it is to be noted that the O(1)−O(2) distance, referring to the strength of the hydrogen bonding between the O atoms of the ($Sb_2O_6^{2-}$) frameworks and the H_2O or H_3O^+ species, is elongated by the yttrium doping. As listed in Table 2, the shortest distance is 2.60 and 2.71 Å, respectively, for the $HSbO_3 \cdot 0.5H_2O$ and $H_{0.64}Y_{0.12}SbO_3 \cdot 0.5H_2O$ compounds. How-

(20) David, R. D., Ed. *CRC Handbook of Chemistry and Physics*; CRC Press: Boca Raton, FL, 1999.

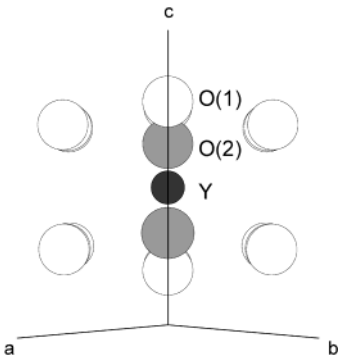

Figure 7. The O(1), O(2), and Y atom positions in the cavity of the yttrium-doped antimonic acid.

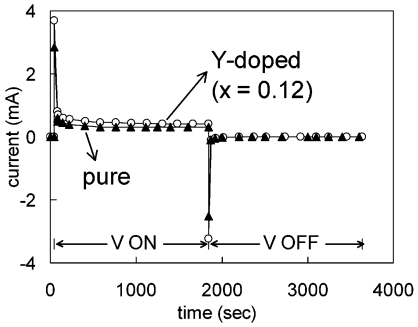

Figure 8. The typical polarization−depolarization curves for the materials ($x = 0$ and 0.12) recorded by applying a 1-V dc bias and cutting it off at the temperature of 20 °C.

ever, as a matter of course, X-ray diffraction alone does not provide the information on the H positions or the quantitative proportions of the H_2O and H_3O^+ species. Further investigations are needed in the future regarding such information,

Ionic Transference Numbers. The ionic transference numbers of the mixed conductors can be determined using a simplified polarization method, for which the introduction of an ion-blocking electrode is regarded as an essential technique.[21] The ionic transference number (t_i) is given by the following equation

$$t_i = \sigma(\text{ion})/\sigma(\text{total}) = 1 - \sigma(\text{electron})/\sigma(\text{total}) = 1 - \sigma(\infty)/\sigma(0) \quad (6)$$

and, because $\sigma(\infty)/\sigma(0) = I(\infty)/I(0)$,

$$t_i = 1 - I(\infty)/I(0) \quad (7)$$

where $I(0)$ and $I(\infty)$ are the dc currents at the initial and infinite times, respectively. In the actual dc measurements, there is usually a time lag between the observed and real values of $I(0)$, and thus, the $I(0)$ values were determined by the ac measurements in this study. Figure 8 shows the typical polarization−depolarization curve for the yttrium-doped antimonic acids ($x = 0$ and 0.12, $n = 0.5$), recorded by applying a 1-V dc bias and cutting it off at the temperature of 20 °C. As shown in Figure 8, the polarization−depolarization curve is clear and symmetrical; the currents reach a steady state within initial tens of seconds during both the polarization and depolarization processes. It was confirmed that such a clear polarization−depolarization curve is also

(21) Vest, R. W.; Tallan, N. M. *J. Appl. Phys.* **1965**, *36*, 543.

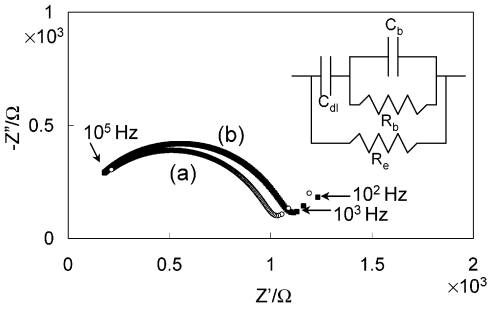

Figure 9. Typical Cole−Cole plots for the materials ($x = 0$ and 0.12) recorded in the frequency range of 10^2−10^5 Hz at the temperatures of 243 and 273 K for $x = 0.12$ and 0, respectively. An equivalent electrical circuit for a homogeneous ionic conductor is also shown. R_b, bulk resistance; C_b, bulk capacitance; C_{dl}, electrode capacitance; R_e, electrical resistance.

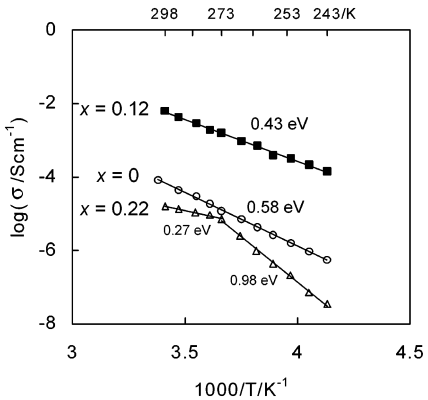

Figure 10. Temperature dependence of the proton conductivity (σ) of the materials ($x = 0$, 0.12, and 0.22) in the temperature range of 243−298 K. The activation energies calculated from the Arrhenius equation are also shown.

observed for the $x = 0.22$ material. All the transference numbers determined from eq 7 were found to be above 0.98, which suggests that the conduction is almost complete ionic proton conduction.

Proton Conductivity. Figure 9 shows the typical complex impedance plots (Cole−Cole plots) for the yttrium-doped antimonic acids ($x = 0$ and 0.12, $n = 0.5$) measured in the frequency region of 10^2−10^5 Hz at the temperatures of 243 and 273 K. In Figure 9, an equivalent electrical circuit for a homogeneous ionic conductor with ion-blocking electrodes is also shown.[22] The plots consist of two parts: a semicircle in the high-frequency region (10^3−10^5 Hz) and a straight line with a slope of 45° in the low-frequency region (10^2−10^3 Hz). Such behavior is consistent with that resulting from the equivalent electrical circuit.

The proton conductivity can be evaluated from the diameters of the semicircles, signifying the bulk resistance and the geometric factors of the disk samples, that is, the electrode areas and thickness. Figure 10 shows the temperature dependence of the proton conductivity (σ) in the temperature range of 243−298 K. In Figure 10, the activation energies (E_a) calculated from the Arrhenius equation are also given. It is obvious that each plot consists of one or two straight lines. Compared with the behavior for $x = 0$ and 0.12, it was found that the proton conductivity for $x = 0.12$ is nearly 2 orders

(22) West, A. R. *Solid State Chemistry and Its Application*; Wiley: New York, 1984.

of magnitude greater than that for $x = 0$ in the investigated temperature range. For example, the proton conductivity at 298 K is 3.8×10^{-3} and 8.3×10^{-5} S cm^{-1}, respectively, for $x = 0.12$ and 0. On the other hand, the activation energy is reduced from 0.58 to 0.43 eV as the x value increases from 0 to 0.12.

For $x = 0.22$, the conductivity at 298 K (1.6×10^{-5} S cm^{-1}) is lower than that for $x = 0$, which suggests that the enlargement of the amorphous material does not contribute to an enhancement in the proton conductivity. The activation energies of 0.98 and 0.27 eV were obtained in the temperature range of 243−273 and 273−298 K, respectively. The high E_a value of 0.98 eV is attributed to the so-called quasifree water freezing, as reported in the $H_3Sb_3P_2O_{14}\cdot nH_2O$ by Deniard-Courant and Piffard.[19] The small E_a value of 0.27 eV suggests that the proton conduction for the $x = 0.22$ material occurs by a surface liquidlike water mechanism.[6,23]

In connection with the enhancement in the proton conductivity observed for $x = 0.12$, it may be pointed out that the O(1)−O(2) distance is elongated as listed in Table 2. Such an elongation may weaken the hydrogen-bond network in the cavity that makes molecular rotation easier, and an easier molecular rotation would reduce the E_a values, as reported for the compounds of $H_5O_2\{M(SO_4)_2\cdot 2H_2O\}$ (M = Fe, In or Tl) by Brach and Goodenough.[24] However, further investigations are needed to fully understand the mechanism.

Conclusions

We have demonstrated the preparation of the yttrium-doped antimonic acids by solution processing using the reaction of antimony and yttrium alkoxides with an aqueous H_2O_2 solution, and the characterization and some electrical properties of these materials. It is recognized that the resulting materials ($x = 0$ and 0.12) consist of fine crystals with an octahedral geometry and that the individual crystals characteristically have a relatively uniform particle size of 40−50 nm. The Rietveld refinement based on the X-ray diffraction data reveals that the Y atoms in the materials are doped into the 16d site of an interstitial site in the cavity. The proton conductivity at 20 °C for the material ($x = 0.12$) is significantly enhanced by about 2 orders of magnitude compared to that for the pure material. Such an enhancement is qualitatively interpreted in terms of the yttrium-doping effect on the strength of the hydrogen bonding between the O atoms of the ($Sb_2O_6^{2-}$) frameworks and H_2O or H_3O^+ species. At present, further investigations are in progress regarding the enhancement in the proton conductivity.

Similar behavior on the structural and electrical properties can also be observed for the bismuth-doped antimonic acids, which will be reported soon.

Acknowledgment. The authors wish to acknowledge Prof. H. Imoto and Dr. Y. J. Shan (Faculty of Engineering, University of Utsunomiya, Japan) for the helpful scientific discussion.

Note Added after ASAP Posting. This article was released ASAP on 1/22/2003 with an error in Table 2. The correct version was posted on 2/4/2003.

CM020990I

(23) Kreuer, K. D.; Rabenau, A. *Appl. Phys. A* **1983**, *32*, 45.
(24) Brach, I.; Goodenough, J. B. *Solid Sate Ionics* **1988**, *27*, 243.